Computers & Industrial Engineering 184 (2023) 109536

Contents lists available at ScienceDirect

Computers & Industrial Engineering

journal homepage: www.elsevier.com/locate/caie

Optimal design of a Low-Cost SAE JA2954 compliant WPT system using NSGA-II

O. García-Izquierdo [a,*], J.F. Sanz [a], J.L. Villa [a], G. Martin-Segura [b]

[a] Instituto Universitario de Investigación Mixto CIRCE Universidad de Zaragoza-Fundación CIRCE, Zaragoza, Spain
[b] Wallbox Chargers, Barcelona, Spain

ARTICLE INFO

MSC:
0000
1111

Keywords:
WPT
NSGA-II
Secant method
Low-cost
SAE J2954

ABSTRACT

Wireless Power Transfer (WPT) systems for electric vehicle charging are one of the most promising methods that, given the advantages they bring, will help the desired deployment of electric vehicles. This paper presents a mathematical optimisation method applied to the design of an 11 kW S-S system that complies with the SAE J2954 standard. A proposal is made to calculate the electrical parameters of the circuit based on equations that are compared with the results obtained by simulation with finite elements and experimental measurements, achieving very tight results with a reduced computational time. The NSGA-II multi-objective genetic algorithm is then applied together with the secant method, defining three different scenarios: minimisation of the primary copper volume, minimisation of the secondary copper volume and a compromise solution optimising the total primary and secondary copper volume. The result is a set of Pareto optimal solutions, from which the one that meets the standard can be extracted that suits the designer's needs.

1. Introduction

Wireless Power Transfer (WPT) systems for electric vehicle (EV) charging are very promising due to their advantages and charging flexibility. These systems support static, opportunity, and dynamic charging, which has attracted considerable interest in terms of design and optimisation. However, the widespread adoption of inductive charging faces two key challenges: the cost of on-board and on-shore components and the need to ensure optimal performance, particularly during opportunity and dynamic charging scenarios.

Inductive power transfer encompasses four classical resonant topologies: S-S, S-P, P-S and P-P (Sallan, Villa, Llombart, & Sanz, 2009). In addition, there are more complex topologies, such as LCC-S, SP-S or LCC-LCC (Aydin, Aydemir, Aksoz, El Baghdadi, & Hegazy, 2022; Chen et al., 2019; Villa, Sallan, Sanz Osorio, & Llombart, 2012), which offer improved performance in cases of misalignment or battery load changes. However, these complex topologies involve a larger number of components, which makes them more expensive. S-S is one of the most widely used today (Aydin et al., 2022) due to its efficiency (Shevchenko et al., 2019; Villa, Sallán, Llombart, & Sanz, 2009; Yang et al., 2023; Yao et al., 2019; Zhang & Mi, 2016) and simplicity, requiring the fewest number of components, as it does not need a filtering coil. In Sallan et al. (2009), Shevchenko et al. (2019) it has been shown that the S-S topology requires less copper than other topologies, coinciding with the main objective of this work, which is to reduce copper volumes and overall cost. In addition, the S-S topology is the only one that allows constant frequency control, as frequency is not affected by coupling conditions such as distance, misalignment or battery voltage.

In terms of the power to be transferred, the SAE J2954 standard classifies charging speed into three categories: WPT 1, 2 and 3, with maximum powers of 3.7 kW, 7.7 kW and 11 kW, respectively (Cirimele et al., 2020; *Wireless Power Transfer for Light-Duty Plug-in/Electric Vehicles and Alignment Methodology*, 2020).

This article focuses on the optimisation of the S-S topology, which offers superior performance with fewer components in the circuit among the classic topologies, using 11 kW as the highest power level defined by the SAE J2954 standard.

The design of WPT systems requires consideration of several parameters, such as resonant topology type, power, coil size, supply voltage, battery voltage, air gap and misalignment, among others. Some parameters are design-specific and cannot be changed, while others can be optimised to achieve the best possible system performance.

The optimisation methods used in WPT systems can be classified according to various parameters, resulting in a broad and complex classification task. This review mainly considers three aspects: the optimised part of the topology, the modelling method employed and the mathematical optimisation technique used.

* Corresponding author.
E-mail address: ogarcia@unizar.es (O. García-Izquierdo).

https://doi.org/10.1016/j.cie.2023.109536
Received 19 April 2023; Received in revised form 19 July 2023; Accepted 10 August 2023
Available online 12 August 2023

In terms of which part of the topology is optimised, three main categories emerge. The first category focuses exclusively on the optimisation of the inductor system, including magnetic flux density (B), primary coil inductance (L_p), secondary coil inductance (L_s), mutual inductance (M), and the possible incorporation of ferrites and aluminium shielding (Luo, Wei, & Covic, 2018; Otomo & Igarashi, 2019; Pei, Pichon, Le Bihan, Bensetti, & Dessante, 2022; Yilmaz, Hasan, Zane, & Pantic, 2017), in this category the optimisation is performed independently of the selected compensator in a next step. The second category involves the optimisation of the primary (C_p) and secondary (C_s) resonant capacitors, as well as other auxiliary components if any, as proposed in Bertoluzzo, Di Barba, Forzan, Mognaschi, and Sieni (2021), Yang et al. (2023), where the capacitors of an LCC-LCC circuit are optimised, and in Yao et al. (2019), for an S-CLC configuration. The third category encompasses the optimisation of both the inductor system and the capacitors. For example, Hasan, Yilmaz, Zane, and Pantic (2015), Sallan et al. (2009) present the optimisation of all classical topologies with different objective functions, in Villa et al. (2012) the S-S and SP-S topologies are optimised and compared. In Bosshard and Kolar (2016), in addition to the S-S topology, the inductor is optimised by means of FEM simulation, as well as the control electronics. In Yan, Yang, He, and Tang (2018), for an S-S topology, the main variables affecting the system are analysed and the inductance with circular shape is optimised. Also Tan et al. (2019) performs an optimisation of an S-S topology by analysing and selecting the most relevant variables through sensitivity analysis.

In all three categories, different optimisation objectives are pursued, such as minimising the copper in both coils (Sallan et al., 2009), optimising the coupling coefficient (k) and B (Luo et al., 2018; Otomo & Igarashi, 2019; Yilmaz et al., 2017), or improving the power transfer efficiency (Bosshard & Kolar, 2016; Yan et al., 2018), among others. Depending on the objective, the different system parameters can be considered fixed or subject to optimisation within specific constraints.

As for the modelling method used, in the case of resonant topology, it is usually modelled mathematically by circuit equations, as in Hasan et al. (2015), Sallan et al. (2009) for all classical topologies, Villa et al. (2012) S-S and SP-S, in Bosshard and Kolar (2016), Tan et al. (2019), Villa et al. (2009) for S-S, Bertoluzzo et al. (2021), Yang et al. (2023) for LCC-LCC or Yao et al. (2019) for a S-CLC. Only one paper has been found that uses a simulator (Yan et al., 2018) instead of circuit equations. Regarding the inductance modelling method (L_s, L_p and M), they can be classified into two types: those using mathematical equations (Sallan et al., 2009; Yan et al., 2018) and those using finite element methods (FEM) (Luo et al., 2018; Otomo & Igarashi, 2019; Tan et al., 2019; Yilmaz et al., 2017). In general, FEM produces more accurate results, but requires much more computational resources, which can limit the inclusion of iterative methods. Consequently, efforts are being made to improve the accuracy of mathematical modelling techniques.

With respect to the optimisation techniques used, these can be classified into two large groups: iterative parameter sweeping methods (Bosshard & Kolar, 2016; Sallan et al., 2009; Yan et al., 2018) and advanced optimisation algorithms such as NSGA-II type genetic algorithms (Bertoluzzo et al., 2021; Luo et al., 2018; Pei et al., 2022; Tan et al., 2019) or particle swarm optimisation (PSO) in both mono and multi objective versions (Hasan et al., 2015; Pei et al., 2022; Yang et al., 2023; Yao et al., 2019; Yilmaz et al., 2017), among others. The following conclusions can be drawn from this preliminary study:

- Advanced optimisation algorithms improve computational speed compared to iterative sweep methods.
- Mathematical modelling of electromagnetic inductances is faster than FEM modelling, although with slightly lower accuracy.
- No significant differences are observed between the different advanced optimisation algorithms.
- The greatest time reduction is achieved by reducing the simulation parameters (Tan et al., 2019) and simplifying the geometry.

The primary motivation of this work is to design a cost-optimised 11 kW S-S WPT system that complies with SAE J2954, along with additional constraints proposed by the designers, such as efficiency greater than 95% and compliance with maximum current and voltage limits on the circuit components. SAE J2954 introduces constraints on frequency and system geometry to ensure interoperability.

The optimal design of compensation coils and capacitors involves numerous variables, requiring the use of 3D finite element programs to accurately calculate the electrical parameters at each iteration, which involves considerable computational effort.

To simplify the computational effort and reduce the execution time, two essential contributions are made. The first consists of modelling the inductance and resistance values of the circuit by means of mathematical equations. The second contribution consists of the development of the NSGA-II multiobjective genetic algorithm for the optimal design of coils and capacitors for the WPT system, according to the proposed objective.

Mathematical equations are proposed to model the inductance and resistance values in the circuit, eliminating the need for 3D finite element programs in each iteration. The results of the equations have been validated by comparing them with results obtained with COMSOL Multiphysics and with experimental measurements, demonstrating comparable values with negligible error. Furthermore, the proposed method significantly outperforms finite element modelling in terms of computational time.

The proposed NSGA-II algorithm establishes two competing objective functions: minimising the copper volume of the primary coil and minimising the copper volume of the secondary coil. In addition, it incorporates a set of constraints according to the SAE J2954 standard and operation constraints of the circuit elements defined by the authors. Three decision scenarios are defined to select the optimal solution according to the manufacturer's interests: minimising the ground copper volume, the on-board copper volume or both simultaneously. The algorithm produces a Pareto optimal set from which the three different optimal designs, one for each scenario, and compliant with SAE J2954, can be extracted. These designs are compared and their performance validated using Matlab-Simulink. The proposed method can be easily adapted to other WPT compensation topologies by modifying the circuit equations and design constraints.

The paper is structured as follows: Section 2 explains the S-S equations of the WPT, defines the parameters set by SAE J2954 and the parameters to be optimised. Section 3 explains the mathematical equations proposed for the electromagnetic modelling of resistances and inductances, comparing them with other methods, such as COMSOL Multiphysics and experimental measurements, also evaluating the required calculation time. Section 4 presents the proposed NSGA-II algorithm, the objective functions, the design constraints and the calculation process. Section 5 discusses the required number of populations and generations to obtain valid results. Section 6 selects the best solution for each scenario and compares them. Finally, Section 7 presents the conclusions, including the verification of the obtained designs using Matlab-Simulink.

2. S-S WPT system to optimise

As indicated in the introduction, in this work the S-S topology is chosen for optimisation, which can be seen in Fig. 1a together with the control electronics proposed in the work as well as its simplification in Fig. 1(b). Movagharnejad and Mertens (2017), Shevchenko et al. (2019), Zhang and Mi (2016)

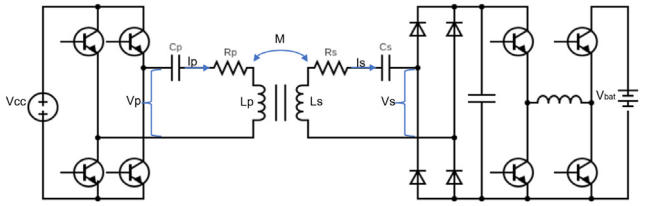

(a) System and proposed electronics

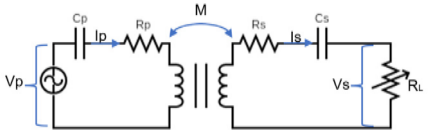

(b) Model of the circuit

Fig. 1. S-S topology.

The following simplifications have been taken into account for the mathematical modelling:

- First harmonic approximation: the input voltage will be considered as a sinusoidal source.
- The resistor R_L models the battery.

Typically, the power electronics used consist of an AC/DC converter and a full bridge on the primary side, with an optional PFC in between. However, in the secondary, the electronics are usually very simple, based mainly on a controllable or non-controllable AC/DC.

In these cases, the battery can be modelled as an equivalent resistor using its voltage (V_{bat}), and the power objective (P_D).

In this paper, it is proposed to use a controllable DC/DC converter in the secondary between the diode bridge and the battery. This converter allows the secondary voltage V_s to be modified independently of the battery voltage V_{bat}, thus providing an additional optimisation variable.

The value of the resistance (R_L) (Cirimele et al., 2020) is obtained from the following:

$$R_L = \frac{8}{\pi^2}\frac{V_s^2}{P_D} \tag{1}$$

Where V_s is the battery voltage set by the DC/DC converter, and is therefore a parameter to be optimised and P_D is a fixed parameter. The equations of the circuit in Fig. 1(b) are:

$$\overline{V_p} = \left(R_p + j\left(L_p w - \frac{1}{C_p w}\right)\right)\overline{I_p} - jwM\overline{I_s} \tag{2}$$

$$0 = \left((R_s + R_L) + j\left(L_s w - \frac{1}{C_s w}\right)\right)\overline{I_s} - jwM\overline{I_p} \tag{3}$$

Being V_p the input voltage, R_p and R_s the primary and secondary resistances respectively, L_p and L_s the primary and secondary inductances, w the angular frequency, I_p and I_s the primary and secondary currents, C_p and C_s the primary and secondary resonant capacitors, M the mutual inductance between inductors. Both equations (2,3) can be combined to obtain the equivalent total impedance (Z_t):

$$\overline{V_p} = \overline{I_p}\left(R_p + j(L_p w - \frac{1}{C_p w}) + \frac{(wM)^2}{R_s + R_L + j(L_s w - \frac{1}{C_s w})}\right) = \overline{I_p Z_t} \tag{4}$$

The primary current I_p is a function of the primary voltage V_p and the impedance Z_t, which depends on R_L and M (4).

Resonance capacitors are obtained from:

$$C_p = \frac{1}{L_p w^2} \tag{5}$$

$$C_s = \frac{1}{L_s w^2} \tag{6}$$

Being the power delivered to the secondary (P_s):

$$P_s = R_L I_s^2 = R_L\left(\frac{wMI_p}{R_p + R_s + j(L_s w - \frac{1}{C_s w})}\right)^2 \tag{7}$$

Which, when working in resonance, is simplified as:

$$P_s = \frac{8}{\pi^2}\frac{V_s^2}{P_D}\left(\frac{wMI_p}{R_p + R_s}\right)^2 \tag{8}$$

The power, under resonance conditions and with low R_s and R_p, is a function of I_p, V_s and M only. Therefore, the power is mainly dependent on V_p, M, V_s, and the frequency.

One of the problems of WPT systems is the high value of the voltages in the capacitors VC_p and VC_s. To minimise their value, they have been taken into account in the optimisation process. These voltages are related to the primary Q_p and secondary Q_s quality factors:

$$VC_p = \frac{I_p}{C_p w} = \frac{I_p}{C_p w}\frac{R_L}{wM^2}\frac{wM^2}{R_L}\frac{I_p}{I_p} = \frac{Q_p P_p}{I_p} = Q_p V_p \tag{9}$$

$$VC_s = \frac{I_s}{C_s w} = \frac{I_s}{C_s w}\frac{R_L}{R_L}\frac{I_s}{I_s} = \frac{Q_s P_s}{I_s} = Q_s V_s \tag{10}$$

Where P_p is the primary power.

To limit these voltages and reduce the number of capacitors in series (Sallan et al., 2009), systems must be designed with low-quality factors. However, reducing the quality factors means reducing the efficiency of the system (Jinliang, Qijun, Wenshan, & Hong, 2017). Instead, it is preferable to work with the values of the input voltage V_p and output voltage V_{bat}. The primary power electronics control the value of V_p. However, V_{bat} is an ineligible value given by the type of battery and its state of charge, so what is considered is that there is a buck-boost in the secondary, able to regulate the voltage at the output of the diode bridge V_s. Therefore V_p and V_s are considered as modifiable values to optimise the system.

Another restriction of the system is stability (Sallan et al., 2009) to avoid the bifurcation phenomenon, for which there must be a single resonance frequency throughout the working range. If this condition is met, the controllability is very predictable and if the working frequency varies, the voltage and current values do not increase, so there is no need for control. On the other hand, it will be unstable when, with a variation of the frequency, any of these values are above the nominal values, which requires precise control to avoid it.

For the system to be stable (Wang, Covic, & Stielau, 2001), the imaginary component of the impedance Z_t must be zero:

$$\left(L_p w - \frac{1}{C_p w}\right) - \frac{w^2M^2(L_s w - \frac{1}{C_s w})}{(R_s + R_L)^2 + (L_s w - \frac{1}{C_s w})^2} = 0 \tag{11}$$

Under these conditions, it is fulfilled:

$$Q_p > \frac{4Q_s^3}{4Q_s^2 - 1} \tag{12}$$

This is considered as the non-bifurcation or stability condition of the system (Wang et al., 2001). Table 1 summarises the mathematical expressions of the S-S circuit under the given design conditions.

The design of any topology defines a set of fixed or non-modifiable design parameters and others that must be calculated to optimise its operation. In the work presented, the fixed design parameters are shown in Table 2. The above fixed parameters are given by the SAE J2954 (*Wireless Power Transfer for Light-Duty Plug-in/Electric Vehicles and Alignment Methodology*, 2020) for the case of a WPT3Z3 coil.

Six parameters, k are considered for optimisation:

- Number of turns of both inductors: N_p, N_s

Table 1
Expressions for the topology studied.

Parameter	Equation
C_p	$\frac{1}{L_p\omega^2}$
C_s	$\frac{1}{L_s\omega^2}$
I_p	$\frac{V_p}{Z_t}$
I_s	$\frac{jwMI_p}{(R_s+R_L)+j(L_s\omega-\frac{1}{C_s\omega})}$
VC_p	$\frac{I_p}{C_p\omega j}$
VC_s	$\frac{I_s}{C_s\omega j}$
η	$\frac{I_s^2R_L}{I_p^2R_p+I_s^2(R_s+R_L)}$

Table 2
Fixed parameters.

Parameter	Value
Inductor	square shaped
a_p (mm)	0.65
b_p (mm)	0.5
a_s (mm)	0.38
b_s (mm)	0.38
Distance between inductors (mm)	0.25
P_D (kW)	11

Table 3
Maximum and minimum values of the parameters to be optimised.

Variable	Minimum	Maximum
S_p (mm^2)	1	80
N_p	1	20
S_s (mm^2)	1	80
N_s	1	20
V_p (V)	300	600
V_s (V)	300	600

- Section of the conductors of both inductors: S_p, S_s.
- Input voltage: V_p.
- Output voltage: V_s.

For all these parameters, maximum and minimum values are defined, as can be seen in Table 3.

For the cable cross-section, the packing factor must be taken into account, in this case a factor of 0.5 (Woodworth et al., 2019) has been considered. On the other hand, the operating frequency is a parameter that must be calculated in such a way as to allow the transfer of the fixed design power P_D. The calculated frequency must be within the range allowed by the Standard: $79 \leq f \leq 90$ kHz.

Neither the ferrites nor the aluminium of the shield shall be taken into account in the design.

3. Electromagnetic modelling

In the circuit of Fig. 1(b), it is necessary to calculate the values of L_s, L_p, M, R_s and R_p; by electromagnetic modelling, where the inductance are independent of the operating frequency, while the resistances depend on the frequency.

Electromagnetic modelling has experienced significant development in recent years due to its wide applications in radio frequency (Aebischer, 2020), RFID-type antennas (Aebischer, 2020), WPT for mobile phone chargers (Low, Chinga, Tseng, & Lin, 2009) and electric vehicles etc. There are basically two options for electromagnetic modelling:

- Simplified modelling using equations, without considering shielding.
- Modelling by means of FEA programs.

The first method gives excellent results when applied to the calculation of coils and capacitors of simplified topologies. It allows very fast computation times, which is crucial when many simulations have to be performed (Aebischer, 2018, 2020; Aebischer & Aebischer, 2014). The second method uses Maxwell's equations, calculating the values of the electromagnetic parameters in a very accurate and precise way, however, its main drawback is that it requires an enormous computational time. Due to the large number of iterations needed to obtain the optimal solution, the first method has been chosen in the present work.

3.1. Modelling of inductances

Three main equation-based modelling methods can be found in the literature:

- Methods based on analytical equations (Aebischer & Aebischer, 2014; Sallan et al., 2009) which give high errors when the number of turns is low (Aebischer, 2019).
- The Greenhouse method (Greenhouse, 1974), which allows obtaining a precise impedance value. It consists of the partial calculation of each section of one turn of the inductor, then adding the mutual impedances according to the direction of the current. The main drawback of this method is that it is difficult to automate in order to include it in iterative processes.
- The third is an intermediate methodology based on the geometric mean distance (GMD). It is derived on the well-known formulation of the inductance of a turn and the mutual inductance between parallel turns (Aebischer, 2019, 2020).

The GMD method is chosen because of its simplicity and the good results obtained. This method has been used (Aebischer, 2020) for rectangular conductors and small coils that are embedded in PCB boards. To use this method for large coils of circular cross-section, which is the case for WPT systems, the circular cross-section area of the inductor is approximated to a rectangular one, defining the diameter d as:

$$d = 2\sqrt{\frac{l_1 l_2}{\pi}} \tag{13}$$

Being l_1 and l_2 the lengths of the square section of the coil.

Thus, the partial self-inductances L_a and L_b of the a and b sides (Table 2) of each coil are obtained from:

$$L_c = \frac{\mu_0 c}{2\pi}\left(\log\left(\sqrt{(c^2 + AMSD_L^2)} + c\right) - \log GMD_L - \sqrt{1+\left(\frac{AMSD_L}{c}\right)^2} + \frac{AMD_L}{c}\right) \tag{14}$$

Where c is the average length of the a or b side of the coil, μ_0 is the magnetic permeability of the vacuum, $AMSD_L$, GMD_L and AMD_L are the compound mean distances belonging to the partial self-inductance of the sides of the single-turn coil, whose calculation method can be seen in Aebischer (2020).

The mutual inductance M_c between the parallel turns of side a at an average mutual distance b, and the mutual inductance M_b between the parallel turns of side b at an average mutual distance a, are given by:

$$M_c = \frac{\mu_0 c}{2\pi}\left(\log\left(\sqrt{(c^2 + AMSD_{\bar{c}}^2)} + c\right) - \log GMD_{\bar{c}} - \sqrt{1+\left(\frac{AMSD_{\bar{c}}}{c}\right)^2} + \frac{AMD_{\bar{c}}}{c}\right) \tag{15}$$

Where c is the average length of the a or b side of the coil and $\bar{c}$ is the average length of the b or a side of the coil. When $c = a$, then $\bar{c} = b$, and vice versa.

Finally, the total inductance of each coil is obtained from the following:

$$L = 2N_i^2(L_a + L_b - (M_a + M_b)) \tag{16}$$

Where L_a and L_b are obtained from Eq. (14), and M_a and M_b from Eq. (15).

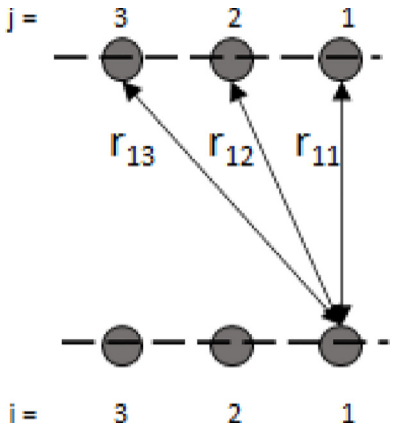

Fig. 2. Example of calculation of mutual inductance M_{ij} according to (18).

3.2. Modelling of the mutual-inductance

The modelling of the mutual inductance is based on the application of the well-known and widely use Neumann expression (17) (Li, Tan, Huang, Wang, & Zhang, 2020; Villa, Llombart, Sanz, & Sallan, 2007):

$$M = \frac{\mu_0}{4\pi} N_p N_s \iint \frac{dl_p dl_s}{r} \tag{17}$$

Where N_p and N_s are the number of turns of the primary and secondary coils, dl_p and dl_s are the infinitesimal integration elements on the contour path of the primary and secondary coils, respectively, and r is the distance between corresponding current elements. In this work, an improvement in the use of the Neumann equation is proposed, particularising the calculation of mutual inductance turn by turn, obtaining the total mutual inductance as the sum of all of them, as seen in (18)

$$M = \sum_{i=1}^{N1}\sum_{j=1}^{N2} M_{ij} = \sum_{i=1}^{N1}\sum_{j=1}^{N2} \frac{\mu_0}{4\pi} \iint \frac{dl_i dl_j}{r_{i,j}} \tag{18}$$

Being M_{ij} the mutual inductance of turn i of the primary concerning turn j of the secondary, as can be seen in Fig. 2

3.3. Modelling of resistors R_p and R_s

Due to the working frequency of the WPT system between 79 and 90 kHz, it is necessary to use a Litz wire to reduce losses, both skin effect P_{skin} and proximity P_{prox} (Acero, Carretero, Lope, Alonso, & Burdío, 2016; Guillod, Huber, Krismer, & Kolar, 2017; Stadler, 2013; Tourkhani & Viarouge, 2001). In order to consider these losses, the resistances of the conductors that allow their modelling R_{skin} and R_{prox}, respectively, are calculated, where R is the total resistivity of the Litz coil:

$$R_i = R_{skin} + R_{prox} \tag{19}$$

The resistance R_{skin} can be modelled (Tourkhani & Viarouge, 2001) with the following expression:

$$R_{skin} = \psi_1(\xi) R_{dc} \tag{20}$$

Where R_{dc} is the DC resistance value and $\psi_1(\zeta)$ is the set of Bessel functions from Eq. (21):

$$\psi_1(\xi) = \frac{ber_0(\frac{\xi}{\sqrt{2}})beri'_0(\frac{\xi}{\sqrt{2}}) - beri_0(\frac{\xi}{\sqrt{2}})ber'_0(\frac{\xi}{\sqrt{2}})}{ber'_0(\frac{\xi}{\sqrt{2}})^2 beri'_0(\frac{\xi}{\sqrt{2}})^2} \tag{21}$$

The Bessel functions allow introducing the variation of the resistance as a function of frequency, where ξ corresponds to the ratio between the strand diameter and the penetration depth.

Table 4
Modelled coils.

Name	Coil 1	Coil 2
Power (kW)	11	11
a (m)	0.65	0.38
b (m)	0.5	0.38
N	15	16
n_t	280	280
d_t (mm)	0.2	0.2
T_d (mm)	1.5	1

Table 5
Inductance comparative.

	L_1 (μH)	Error %	L_2 (μH)	Error %
Proposed (16)	203.68	0.4	112.67	1.82
Based on (Sallan et al., 2009)	296.47	46.14	171.16	54.67
COMSOL	201.96	−0.45	110.8	0.13
Experimental	202.87	–	110.66	–

In the same way, *Rprox* (Tourkhani & Viarouge, 2001) can be obtained through the expression:

$$R_{prox} = \frac{P_{prox}}{I^2} = -\frac{2\sqrt{2}\pi\varphi}{\delta}\frac{H^2}{I^2}\psi_2(\xi) \tag{22}$$

Where φ is the resistivity of the material, δ is the penetration depth, H is the intensity of the magnetic field and $\psi_2(\xi)$ is the set of Bessel functions that considers the effect of frequency using Eq. (23).

$$\psi_2(\xi) = \frac{ber_2(\frac{\xi}{\sqrt{2}})ber'_0(\frac{\xi}{\sqrt{2}}) + beri_2(\frac{\xi}{\sqrt{2}})bei'_0(\frac{\xi}{\sqrt{2}})}{ber^2(\frac{\xi}{\sqrt{2}})beri^2(\frac{\xi}{\sqrt{2}})} \tag{23}$$

3.4. Electromagnetic modelling verification

The validation of the modelling outlined in the previous points is carried out by comparing the results of the following:

- Proposed equations:
  - Based on Aebischer (2020) and adapted to round section for the calculation of L_p and L_s (16).
  - Particularising the Newmann expression for the calculation of M (18).
  - Based on Tourkhani and Viarouge (2001) for the calculation of R_p and R_s (19).
- Modelling equations from Sallan et al. (2009) for calculating L_p and L_s.
- Neumann's expression for calculating M (17).
- Modelling with Comsol Multiphysics for calculating L_p, L_s, M, R_p and R_s.
- Actual measurement of L_p, L_s, M, R_p and R_s, using a GW INSTEK LCR 6300.

The characteristics of the modelled coils can be seen in Table 4.

Being a and b the outer sides of the rectangular coils, N the number of turns, n_t the number of strands, d_t the strand diameter and T_d the separation between turns.

Fig. 3 shows the assembly and the modelling carried out using COMSOL Multiphysics.

3.4.1. Validation of inductances calculation

The results obtained can be seen in Tables 5 and 6.

The absolute error of each case is calculated by comparing it with the measured value using the LCR.

As can be seen, the proposed methods have an error similar to that obtained with finite element modelling and much lower than that obtained using the equations presented in Sallan et al. (2009) and slightly better than the Newmann expression for M.

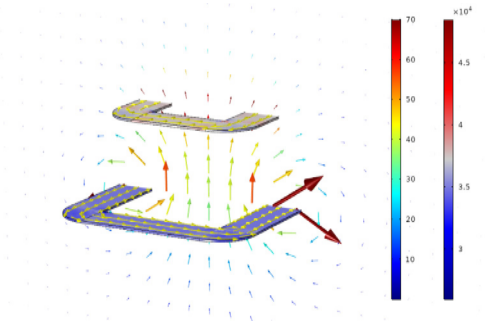

(a) COMSOL Multiphysics model showing magnetic field magnitude and current density

(b) Experimental set-up

Fig. 3. Comparison between experimental set-up and modelling.

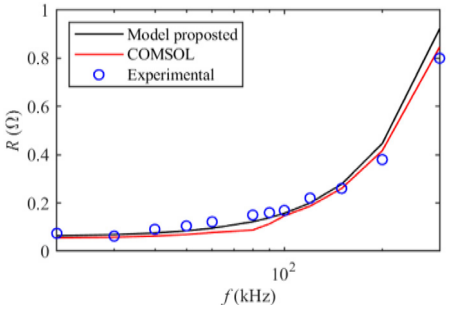

(a) Coil 1

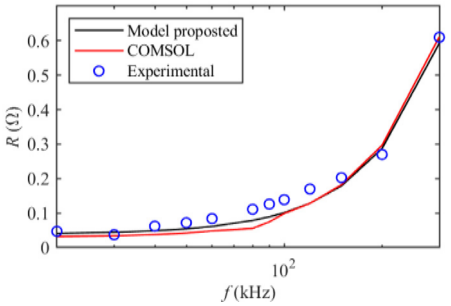

(b) Coil 2

Fig. 4. Resistor of modelling coils.

Table 6
Mutual inductance comparative.

	M (μH)	Error %
Proposed (18)	19.67	0.87
Based on (21)	19.14	1.84
COMSOL	19.36	0.72
Experimental	19.5	–

Table 7
Computation time comparison (seconds).

	L_i	M	R_i
Proposed	0.000116	0.002730	0.002727
COMSOL	30	30	77

3.4.2. Validation of resistances calculation

It has been shown that the value of the resistors depends on the frequency. For this reason, Fig. 4 shows the results obtained as a function of the frequency.

Since COMSOL Multiphysics does not include the possibility of directly calculating the resistance, the method described in Acero et al. (2016) has been implemented. As can be seen in Fig. 4, Eq. (19) gives results practically identical to those obtained with COMSOL Multiphysics and very close to those obtained by measurement with the LCR.

3.4.3. Computation time comparison

The calculation time in iterative processes is a fundamental element for decision-making regarding the modelling to select. In the case of the NSGA-II genetic algorithm proposed in this paper, there are hundreds of iterations of thousands of different points, each with a different inductance and resistance value. In addition, as will be seen in Section 4, the frequency is a parameter calculated by an iterative process that requires, at each step, the calculation of the resistances, making the number of iterations more significant than that of the inductances.

An I9-9900k, 3.6 GHz, 65 GB RAM computer has been used. Table 7 shows the time required to obtain the results in Tables 5 and 6 and Fig. 4, using the proposed equations compared to COMSOL Multiphysics.

As can be seen, the calculation time with COMSOL Multiphysics is tens of thousands of times higher than that required with the proposed equations. Therefore, using the proposed equations in the iterative process is perfectly justified, considering the results' precision.

4. Optimisation methodology

As already explained, the objective is to obtain the cheapest WPT system that meets the design restrictions. Since ferrite and shielding are not considered, Litz coils copper gives the cost, the smaller the volume the lower the cost, so the objective is to minimise the volume of copper in the coils. Since there are two coils, there are two objective functions to minimise, given by the copper volume of each coil:

$$Vol_{cup} = \frac{d_{0p}^2}{4}\pi n_{tp} N_p 2(a_p + b_p) \tag{24}$$

$$Vol_{cus} = \frac{d_{0s}^2}{4}\pi n_{ts} N_s 2(a_s + b_s) \tag{25}$$

Where Vol_{cu} is the volume of copper in each inductor, a and b are the average coil size, n_{ts} is the number of strands, and d_0 is the

Table 8
Limits of the problem.

Parameter	Minimum	Maximum
$Freq$ (kHz)	79	90
Efficiency	95%	–
VC_p (kV)	–	3.5
VC_s (kV)	–	3.5
δ_p (A/mm^2)	–	4
δ_s (A/mm^2)	–	4
L_{cup}	$\frac{R_p+R_s}{3} I_s^2$	–
L_{cus}	$\frac{R_p+R_s}{3} I_p^2$	–
Q_p		$\frac{4Q_s}{4Q_s^2-1}$

strand diameter. For the working frequency between 79 and 90 kHz, the optimum strand diameter is 0.1 mm (Li et al., 2020).

In addition to the previous equations, a set of constraints is included to ensure that the results obtained are within acceptable values. These restrictions are the stability condition, the frequency limits, the minimum value of efficiency, the maximum voltages of the capacitors, the maximum density of the current (Paul, 2018) and an equal distribution of losses between both coils (L_{cup}) and (L_{cus}). Table 8 shows the values considered in the restrictions.

$$J_p = Vol_{cup} + K^2(\Delta Freq + \Delta Eff + \Delta VC_p + \Delta R_p I_p + \Delta\delta_p) \tag{26}$$

$$J_s = Vol_{cus} + K^2(\Delta Freq + \Delta Eff + \Delta VC_s + \Delta R_s I_s + \Delta\delta_s) \tag{27}$$

These restrictions are included in objective functions, which are as follows:

Where:

$$\Delta Freq = \begin{cases} 1 & \text{if } freq < 79 \text{ kHz} \\ 0 & \text{if } 79 \text{ kHz} \le freq \le 90 \text{ kHz} \\ 1 & \text{if } freq > 90 \text{ kHz} \end{cases} \tag{28}$$

$$\Delta Eff = \begin{cases} 1 & \text{if } Efficiency < 95\% \\ 0 & \text{if } Efficiency \ge 95\% \end{cases} \tag{29}$$

$$\Delta VC_i = \begin{cases} 0 & \text{if } VC_i < 3.5 \text{ kV} \\ 1 & \text{if } VC_i \ge 3.5 \text{ kV} \end{cases} \tag{30}$$

$$\Delta\delta_i = \begin{cases} 0 & \text{if } \delta_i < 4 \\ 1 & \text{if } \delta_i \ge 4 \end{cases} \tag{31}$$

$$\Delta L_{cui} = \begin{cases} 0 & \text{if } R_i I_i^2 < \frac{R_p+R_s}{3} I_j^2 \\ 1 & \text{if } R_i I_i^2 < \frac{R_p+R_s}{3} I_j^2 \end{cases} \tag{32}$$

Being K a constant of a high value to penalise solutions that do not meet the constraints. In addition, it is squared to avoid very abrupt transitions. In the case of the presented work, $K = 2E9$.

In the case of resistors, the condition is that the losses in the coils are distributed in such a way that one does not exceed the other by two thirds. In this way, solutions where the losses are very unbalanced are discriminated, avoiding high heating in one of the inductors.

The objective of this optimisation method is to achieve the system that requires the least amount of copper. For this purpose, three decision scenarios are considered:

- Scenario 1: Minimisation of copper from the shore coil (best for the shore coil manufacturer).
- Scenario 2: Minimisation of copper from on-board coil (best for on-board coil manufacturer).
- Scenario 3: Balanced joint copper minimisation of both coils (compromise solution).

Since this is a problem with two competing objective functions to be solved subject to a set of constraints, a multi-objective generic algorithm (MOEA) is needed to find the set of optimal solutions that will form the Pareto Front, the inclusion of elitism in this algorithms improves their performance. Among the most widely used algorithms are Pétrowski and Ben Hamida (2017) NSGA-II, SPEA, SPEA2, PAES MOMGA and MOMGA-II.

The NSGA-II algorithm has been selected because it is the most widely used and cited multi-objective algorithm in the literature (Ma, Zhang, Sun, Liu, & Shan, 2023; Verma, Pant, & Snášel, 2021) with good results. Specifically, this algorithm has been used, in its basic, modified or hybridised version, to solve multiple problems in all types of electrical engineering applications, both in optimal asset location and design and even in the determination of control parameters, such as, for example: in Shahryari, Shayeghi, and Moradzadeh (2018) is used to decide the optimal placement of D-STACOMS in a distributed generation power grid, in Zhang et al. (2019) for the optimal design of a hybrid solar-wind-battery power generation system to supply the power demand of DC facilities and AC cooling equipment of a mobile base station on a small remote island, Wang, Li, Ding, Cheng, and Buja (2023) proposes a parallel DC power system planning method as a demand-side management method to maximise stability gain, economic benefits and RES penetration, In Heydari et al. (2023) an intelligent photovoltaic power output forecasting (PV-OP) model is developed, in Blažek, Prokop, Misak, Kedron, and Pergl (2023) the power consumption in home microgrids with V2G is optimised, in Abid, Ahshan, Al-Abri, Al-Badi, and Albadi (2023) a simultaneous optimal solution technique for distributed renewable generation and the sizing and placement of virtual synchronous generators in distribution grids is proposed, in Balasubramanian et al. (2023) it is used for the optimal design of the permanent magnet inner motor of an EV, Ranjan and Mishra (2015) uses it for the optimal design of a three-phase squirrel cage asynchronous motor, in Mohammadi, Trovão, and Antunes (2020) it optimises the design of a hybrid synchronous excitation machine for electric vehicles, depending on the hybridisation ratio and minimising the material cost, in Ding, Yang, and Xiong (2021) it is used for the optimal design of a traction transformer for high-speed trains, in Abunike, Okoro, and Davidson (2021), El-Nemr, Afifi, Rezk, and Ibrahim (2021) a three-phase four-pole switched reluctance motor (SRM) is optimally designed, in Liu, Wei, Cai, and Yuan (2020) proposes an optimal design method for the 315 kVA three-phase amorphous metal distribution transformer, in Xu, Zhu, Zhang, Zhang, and Quan (2021) proposes the optimal design of a dual-stator linear rotating permanent magnet generator (DSLRPM) with Halbach PM array for marine energy harvesting, in Pan and Fang (2022) uses the algorithm to find the optimal solution to the combination of structural parameters and obtain the optimal efficiency of a permanent magnet arc motor with hybrid dual-stator excitation, in Wang, Han, Chen, Song, and Yuan (2022), the volume and efficiency of the coil of a high frequency transformer is optimised considering the use of different core materials, in Ahmed, Zhu, Yu, and Luo (2022) the algorithm is used to optimise the design of two different Striling motors, minimising the losses and increasing the useful power, in Li and Xia (2021) the algorithm is used for the design of a nonlinear active disturbance rejection control of an S-S WPT, improving the robust behaviour of the system against coupling coefficient or load disturbances, limiting the overshoot within a certain range, and reducing the rise time and steady state error.

The multi-objective optimisation methodology presented is based on the application the NSGA-II (Beyer & Deb, 2001) algorithm to the calculation of the WPT system under study.

A multi-objective optimisation seeks to obtain a set of solutions that, complying with a set of constraints, simultaneously optimise a set of objective functions, which may be opposite.

In this way, a multi-objective optimisation problem is characterised by having two or more opposing objectives, which must be minimised or maximised simultaneously, satisfying certain constraints. In general, this type of multi-objective problem is formulated as follows: Minimise.

$$J(x_i) = (J_1(x_i), J_2(x_i), \dots, J_n(x_i)) \tag{33}$$

$$Over\ x_i \in X \tag{34}$$

Subject to:

$$g(x_i) < 0 f = 1, \ldots, l \tag{35}$$

$$h(x_i) = 0 k = 1, \ldots, m \tag{36}$$

Where:

- $n \geq 2$ is the number of objective functions.
- $x_i = (x_1, x_2, \ldots, x_k)$ is the vector of decision variables.
- X is the space of feasible solutions.
- $J(x_i)$ is the target vector.

In this type of problem, finding an ideal solution capable of optimising all objective functions is impossible. However, it is possible to find a set of non-dominant solutions known as the Pareto Optimal Set, from which a solution relative to the selected scenario can be selected.

The iterative process that has been designed can be seen in Fig. 5. It consists of the following steps:

- Step 1: random initialisation of the population.
- Step 2: mathematical modelling of the system and calculation of objective functions.
- Step 3: evaluation of solution using the Non-dominance test and Crowding distance.
- Step 4: tournament selection.
- Step 5: obtaining the offspring using crossover and mutation operators.

Once the offspring O is obtained in step 5, it is sent to Step 2, while the parents p are sent to Step 3. The process ends when the maximum number of generations defined is reached (Fig. 5).

Step 1: random initialisation of the population

It consists of the random generation of N vectors of decision variables $x_{0,i} \in X_0$; each vector is an individual from the population. The set of values k defines each vector x_i corresponding to the parameters to be optimised (Table 3): $N_p; N_s; S_p; S_s; V_p; V_s$.

$$x_{0,i}(N_p, S_p, V_p, N_s, S_s, V_s) = x_{0,i}(k_l) \in X_0; k = N, S, V; l = p, s \tag{37}$$

Step 2: mathematical modelling of the system and calculation of objective functions J_p and J_s

The main objective of this step is to obtain the values of the objective functions J_p and J_s for each of the individuals generated in Step 1; this is done following the process that can be seen in Fig. 5 and explained below:

Step 2.1 mathematical calculation of the inductances L_p, L_s and M

For each vector x_{p0i} from the Step1, the value of L of each coil and M is calculated by applying Eqs. (16) and (18) respectively. These values are introduced into the vector x_{p0i} obtaining an expanded vector $x_i \in X_0$:

$$x_i(N_p, S_p, V_p, N_s, S_s, V_s, L_p, L_s, M); x_i \in X_0 \tag{38}$$

Step 2.2 Calculation of the circuit parameters that meet the design power $P_D = 11$ kW

To calculate the circuit capable of delivering the design power, it is necessary to obtain the values of R and C for each vector x_i. R and C depend on the frequency. This implies an iterative process until finding the frequency f_i^P for each x_i, giving the set of vectors $x_{f_i^P,i} \in X_{f^P}$ that satisfies the design power condition $P_D = 11$ kW. The iterative process used is the secant-method one.

$$\Delta P_f = P_f - P_D = 0 \tag{39}$$

The secant method is a root-finding algorithm that uses a sequence of roots of secant lines to best approximate the root of a function J. This method reduces the computational cost since it does not need the evaluation of the derivative, as happens with the Newton-Raphson method. For this reason, it is convenient when it has to be used many times. This method estimates the tangent by an approximation. The general equation of the secant method is as follows:

$$x_{k+1} = x_k - \frac{x_k - x_{k-1}}{J(x_k) - J(x_{k-1})} J(x_k) \tag{40}$$

Step 2.2.1 Initialisation of secant method values

In the proposed example, this method is applied starting from the values of maximum frequency (f_{max}) and minimum frequency (f_{min}) as initial values. Applying it to each vector x_i from step 2.1, two decision vectors are obtained for each original vector:

$$x_{fmax,i}(f_{max}, N_p, S_p, V_p, N_s, S_s, V_s, L_p, L_s, M, R_{pfmax}, R_{sfmax}, C_{pfmax}, C_{sfmax}, P_{fmax}) \tag{41}$$

$$x_{fmin,i}(f_{min}, N_p, S_p, V_p, N_s, S_s, V_s, L_p, L_s, M, R_{pfmin}, R_{sfmin}, C_{pfmin}, C_{sfmin}, P_{fmin}) \tag{42}$$

Where

- R_{pfmax}, and R_{pfmin}, are the resistances of the primary coil for f_{max} and f_{min}.
- R_{sfmax}, and R_{sfmin}, are the resistances of the secondary coil for f_{max} and f_{min}.
- C_{pfmax}, and C_{pfmin}, are the capacitors of the primary coil for f_{max} and f_{min}.
- C_{sfmax}, and C_{sfmin}, are the capacitors of the secondary coil for f_{max} and f_{min}.

The values of the resistors are calculated with Eq. (19), while the capacitors are obtained with Eqs. (5) and (6).

Step 2.2.2 secant-method iterative process

In the case of the problem, the first equation used is:

$$f_i^1 = f_{max} - \frac{f_{max} - f_{min}}{\Delta P_{fmax} - \Delta P_{fmin}} \Delta P_{fmax} \tag{43}$$

Being:

$$\Delta P_{fmax} = P_{fmax} - P_D \tag{44}$$

$$\Delta P_{fmin} = P_{fmin} - P_D \tag{45}$$

With $P_D = 11$ kW (Table 2)

The general equation for the iterative process is:

$$f_i^{k+1} = f_i^k - \frac{f_i^k - f_{min}}{\Delta P_{f_i^k} - \Delta P_{fmin}} \Delta P_{f_i^K} \tag{46}$$

This equation is calculated iteratively starting with each pair of initial points, x_{fmax} and x_{fmin}, until obtaining the value of the frequency (f_i^P) at which it is possible to deliver $P_D = 11$ kW. For this, in each iteration, it is necessary to recalculate the parameters that depend on the frequency: R_{pf}, R_{sf}, C_{pf}, C_{sf}, P_f

$$x_{f_i^k,i}(f_i^k, N_p, S_p, V_p, N_s, S_s, V_s, L_p, L_s, M, R_{pf_i^k}, R_{sf_i^k}, C_{pf_i^k}, C_{sf_i^k}, P_{sf_i^k}) \in X_{fk} \tag{47}$$

Once finished, the set of solution vectors $x_{f_i^P,i}$, capable of achieving the design power P_D, is obtained.

$$x_{f_i^P,i}(f_i^P, N_p, S_p, N_s, S_s, V_p, V_s, L_p, L_s, M, R_{pf_i^P}, R_{sf_i^P}, C_{pf_i^P}, C_{sf_i^P}, P_D) \in X_{fP} \tag{48}$$

Step 2.3 Calculation of the objective functions

In this step the objective functions J_p (26) and J_s (27) are calculated including the constraints from the restrictions Table 8.

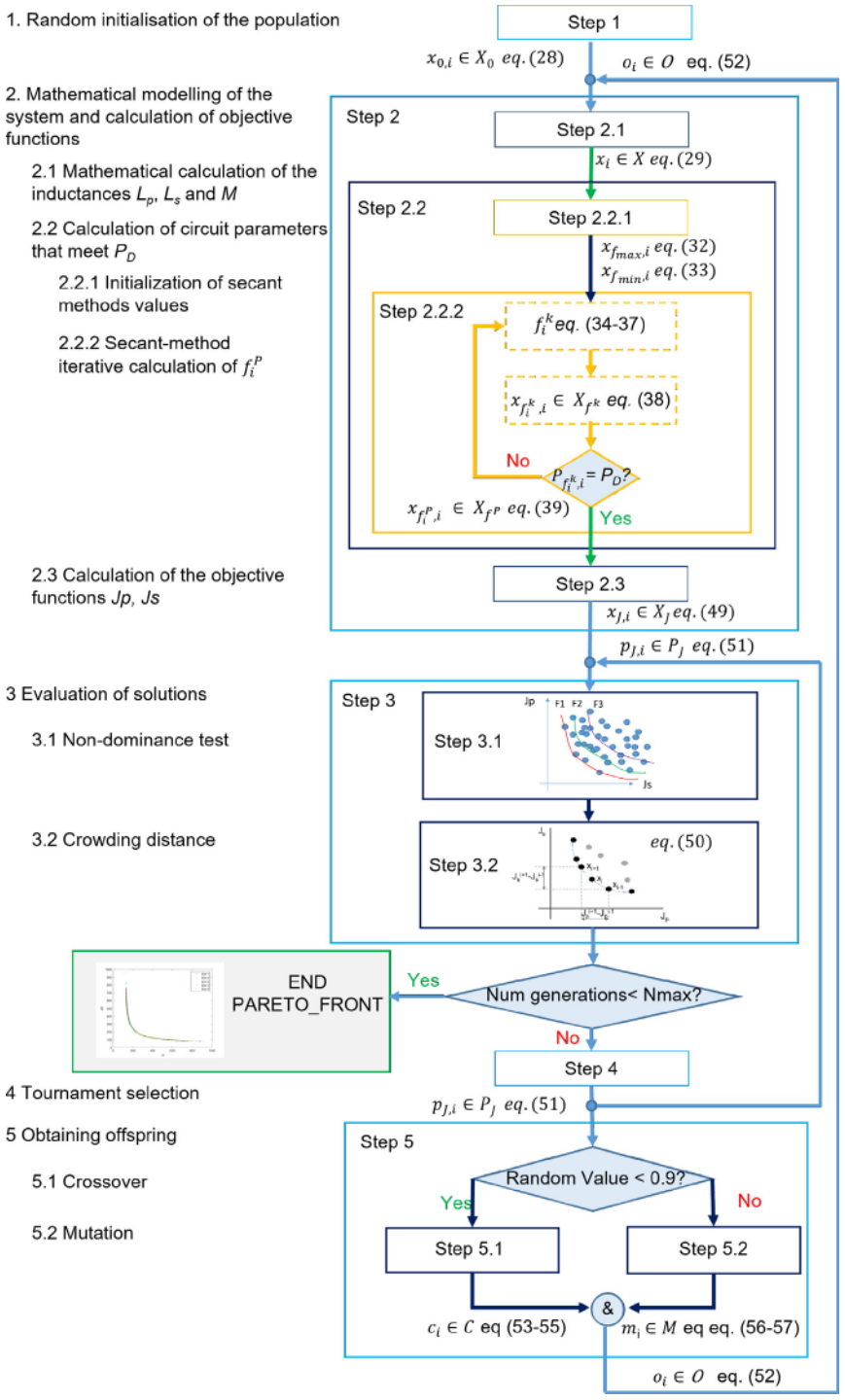

Fig. 5. Algorithm workflow.

At the end of this process, a set of solutions ($x_{J,i} \in X_J$) are obtained, which comply with the defined restrictions:

$$x_{J,i}(f_i^P, N_p, V_p, S_p, N_s, S_s, V_s, L_p, L_s, M, R_{pf_i^P}, R_{sf_i^P}, C_{pf_i^P}, C_{sf_i^P}, P_D, Jp_{f_i^P}, Js_{f_i^P}) \in X_J \quad (49)$$

These solutions are represented as a function of their objective functions J_p and J_s in Fig. 7(a).

Step 3: Evaluation of solutions

Once the set of solutions has been obtained, it is necessary to give them a value that allows the best ones to be distinguished. To do this, two processes are carried out. The first, called the non-dominance test, sorts the solutions into different Pareto-optimal sets. The second, on the other hand, allows us to evaluate the solutions of the same Pareto-optimal set by calculating the crowding distance.

Step 3.1 Non-dominance test

In a single-objective optimisation problem, the superiority of a solution over other solutions is easily determined by comparing their objective function values. In a multi-objective optimisation problem, dominance determines the goodness of a solution. The dominance test is used to compare the results obtained in the Step 2.3; this is based on

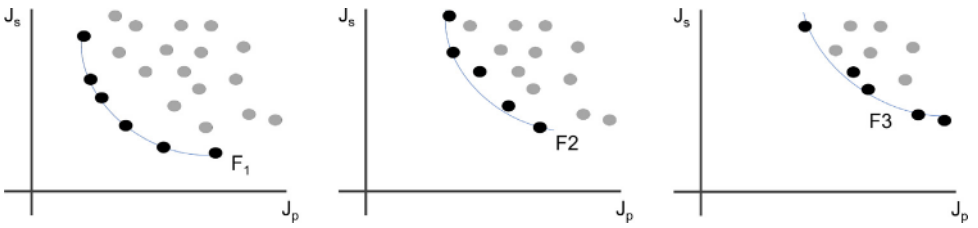

Fig. 6. Obtaining three Pareto-optimal sets F1, F2, F3.

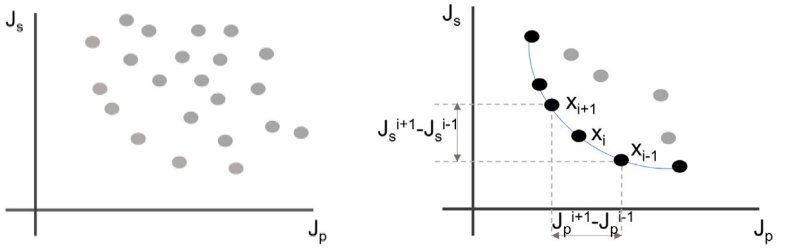

(a) Solutions objective (b) Crowding distance of x_i

Fig. 7. NSGA-II figures.

the fact that a solution x_1 dominates x_2 when the following conditions are met (Deb, Pratap, Agarwal, & Meyarivan, 2002):

- Solution x_1 is not worse than x_2 in all objectives.
- Solution x_1 is strictly better than x_2 in at least one objective.

The dominance process is performed iteratively with each individual in the solution set, obtaining the Non-Dominated Solution Set, composed of all the solutions that are not dominated by any member of the solution set. The non-dominated set of the feasible decision space is called the Pareto-optimal set, and the boundary defined by the set of all mapped points of the Pareto-optimal set is called the Pareto-optimal front.

Multi-objective algorithms try to find as many solutions as possible belonging to the Pareto-optimal front and as diverse a set of solutions as possible. The non-dominated solutions are temporarily eliminated to obtain other rankings, and the procedure is applied again, obtaining a new set of second-level non-dominated solutions. This process can be repeated until all members of the population are ranked within a Pareto set. In the case of the presented work, the procedure is applied several times; obtaining a set of Pareto-optimal fronts (Fig. 6).

Step 3.2: Determine Crowding Distance

The selected solutions of each Pareto front are ordered according to the crowding distance. The objective is to find the Euclidean distance between each solution of the same Pareto front according to its objectives, i.e. to select those whose distance between them is more significant. Solutions located at the extremes of the Pareto set are assigned an infinite distance so that they are always selected.

The equation that defines the Crowding distance is:

$$d_{X,i} = \sum_{m=1}^{2} \left| \frac{J_m(x_{i+1}) - J_m(x_{i-1})}{(J_m^{max} - J_m^{min})} \right| = \left| \frac{J_p(x_{i+1}) - J_p(x_{i-1})}{(J_p^{max} - J_p^{min})} \right| + \left| \frac{J_s(x_{i+1}) - J_s(x_{i-1})}{(J_s^{max} - J_s^{min})} \right| \quad (50)$$

Where: J_m^{max} and J_m^{min} are the maximum and minimum values of the Objective Functions, $J_m(x_{i+1})$ and $J_m(x_{i-1})$ are the neighbouring solutions to x_i, for each objective function J_p and J_s. See Fig. 7(b).

Step 4: Tournament selection

In tournament selection, two comparisons are made. First, the solution located in the best Pareto Set is selected; second, if the solutions belong to the same Pareto Set, the best crowding distance is used to determine the winning solution. The set of solutions obtained is the set of Parents $p_{J,i} \in P_J$, where:

$$p_{J,i}(N_p, S_p, V_p, N_s, S_s, V_s) = p_{J,i}(k_l) \in P_J \quad (51)$$

Step 5: Obtaining offspring

Once the set of parents ($p_{J,i} \in P_J$) has been obtained, the offspring is obtained by crossover ($c_i \in C$) in the Step 5.1 and mutation ($m_i \in M$), in the Step 5.2. Selection between both is carried out probabilistically by means of a uniform function that prioritises crossover over the mutation. The union of the set obtained by crossing and the set obtained by mutation gives as a result the offspring set (O).

$$O = C \cup M \quad (52)$$

At the end of Step 5, the total number of the population of parents (P_J) and offspring (O) is $2N$.

The set of offspring is sent to Step 2 and from there to Step 3. The set of parents, however, is sent directly to Step 3, as there is no need to recalculate the electrical model of the WPT system.

At the output of Step 3, it is checked whether the number of iterations has reached the maximum value. If not, the data is sent to Step 4 and the iterative process continues, otherwise, at the output of Step3, the desired Pareto Front is obtained.

Step 5.1: Crossover offspring

The crossover is based on a Simulated Binary Crossover (SBX) (Beyer & Deb, 2001; Deb & Agrawal, 1995; Raghuwanshi, Kakde, & Gandhi, 2004), for which two different parents of P_J, are randomly chosen, generating two children: c_i, c_{i+1}, whose optimisation variables (k_l) are calculated as follows:

$$c_i(k_l) = \frac{1}{2}((1 - \beta_k)p_{J,i}(k_l) + (1 + \beta_k)p_{J,j}(k_l)) \quad (53)$$

$$c_{i+1}(k_l) = \frac{1}{2}((1 + \beta_k)p_{J,i}(k_l) + (1 - \beta_k)p_{J,j}(k_l)) \quad (54)$$

The process of generating the child values is based on a probability distribution. This distribution controls the spread factor β defined as the ratio of the dispersion of the child values to the parent values, calculated for each variable k_l as follows (Chacón & Segura, 2018):

$$\beta = \begin{cases} (2u)^{\frac{1}{\eta_c+1}} & \text{if } u \le 0.5 \\ \frac{1}{2(1-u)^{\frac{1}{\eta_c+1}}} & \text{if } u > 0.5 \end{cases} \quad (55)$$

Where u is a random value between 0 and 1, and η_c is the distribution index, defined by the user. The distribution index modifies the exploration capability. A low index increases the probability of generating child values that are distant from the parent values, while higher indices result in solutions that closely resemble the parents. The effect of this parameter on the results is analysed in Deb and Kumar (1995), Jung, Choi, and Kim (2017), Sinha (2011b), Zhang, Moreira, and Corte-Real (2015), where in general $\eta_c = 20$ is a value that gives good results and is adopted in this paper.

Step 5.2: Mutation offspring

The mutated offspring is obtained by calculating each optimisation variable for each individual using the following polynomial expression:

$$m_i(k_l) = p_{J,i}(k_l) + (k_{l,max} - k_{l,min})\delta_k \tag{56}$$

With $k_{l,max}$ and $k_{l,min}$ the maximum and minimum values of each optimisation variable k_l defined in the Table 3.

This distribution controls the spread factor δ is calculated for each variable k_l as follows:

$$\delta = \begin{cases} (2r_k)^{\frac{1}{\eta_c+1}} & \text{if } r_k \leq 0.5 \\ 1-(2(1-r_k))^{\frac{1}{\eta_c+1}} & \text{if } r_k > 0.5 \end{cases} \tag{57}$$

Being r_k a value obtained as a uniform function between (0 and 1), and $\eta_c = 20$ is the distribution index.

5. Result and discussion

In the case of evolutionary multi-objective optimisation (EMO) algorithms, the ability to produce solutions that are ideally optimal and uniformly distributed over the entire Pareto front, so that a complete representation is obtained, is often referred to as convergence (Sinha, 2011a).

In general, second generation multi-objective algorithms based on Pareto dominance, which introduce elitism, such as NSGA-II, PAES or SEPA2 show good convergence for two or three objective functions (Pétrowski & Ben Hamida, 2017), specifically in the NSGA-II algorithm, it is found that elitism accelerates and guarantees convergence to the true Pareto optimal set (Ma et al., 2023). Also, a comparison of NSGA and NSGA with elitism and a study of how it affects the number of populations and generations is made in Zitzler, Deb, and Thiele (2000), concluding that elitism clearly improves the performance of the algorithm in the same way as increasing the number of populations and generations.

The performance evaluation of multi-objective optimisation algorithms in Zitzler et al. (2000) is based on three fundamental aspects:

- The distance of the resulting nondominated set to the Pareto-optimal front should be minimised.
- A good (in most cases uniform) distribution of the solutions found is desirable. The assessment of this criterion might be based on a certain distance metric.
- The extent of the obtained nondominated front should be maximised, i.e., for each objective, a wide range of values should be covered by the nondominated solutions.

In Pétrowski and Ben Hamida (2017), Tan, Lee, and Khor (2001), Zitzler, Brockhoff, and Thiele (2007), Zitzler et al. (2000) different ways of performance evaluation are proposed, in addition to the visual analysis (Zitzler et al., 2000) of the obtained Pareto front.

For the case studied, a series of simulations have been carried out taking a population of 100, 500, 1000 and 2000 individuals, allowing for Generations of 100, 500, 1000 and 2000 individuals for each population group. Some of them can be seen in Fig. 8

As expected, the higher the population and Generation, the better the convergence of the solution. By visual inspection, it is observed

Table 9
Average Hypervolume and average number of solution.

Population	Generations	Hypervolume	Num solutions
100	100	0.03139	31.25
100	1000	0.1963	31
1000	100	0.2604	168.5
500	500	0.1996	181.6
1000	1000	0.3225	317
2000	2000	0.3311	606

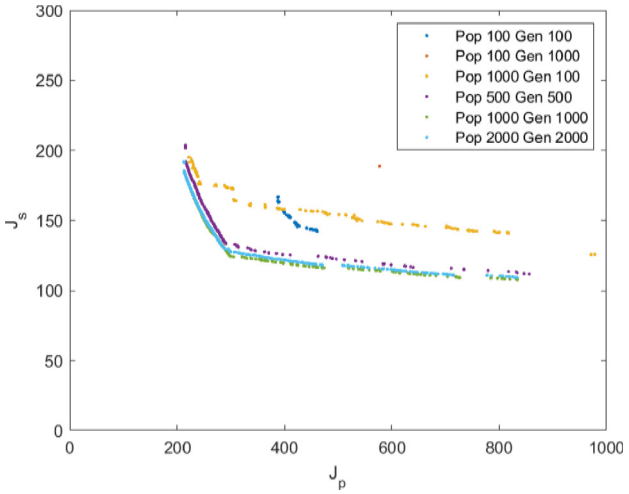

Fig. 8. Pareto-sets obtained for different number of individuals of Population and Generations.

that from $Pop = 500$, $Gen = 500$ the Pareto Fronts are very similar. In addition to the visual analysis, the Hypervolume of the Pareto fronts obtained in the different cases studied has been calculated. Hypervolume provides a quantitative measure of the quality of the Pareto front obtained by a multi-objective algorithm (Tan et al., 2001),(Zitzler et al., 2007). It is calculated by taking the area or volume covered by the Pareto front in the target space. The higher the Hypervolume, the better the quality of the Pareto front, as it indicates better coverage and diversity of solutions. The maximum value of the Hypervolume depends on the dimensionality of the objective space and the distribution of non-dominated solutions, as well as being influenced by the specific characteristics of the problem and the known optimal solutions. Hence, Hypervolume is a relative metric to compare different Pareto fronts or to assess the improvement in the quality of the Pareto front as a multi-objective evolutionary algorithm is executed. The Table 9 shows the average Hypervolume values for the five simulations of the sis analysed population and generation.

Obviously, the larger the population and generation, the more valid solutions are obtained.

It is also observed that in general, it is more efficient to increase the population than the generation, this is due to the fact that the result of the problem is very dependent on the result obtained in the initial iteration, given by the population.

On the other hand, the larger the number of population and generations, the longer the computation time required. As an example, the case of $Pop = 100$, $Gen = 100$ requires only 4 to 5 s, while the case of $Pop = 2000$, $Gen = 2000$ requires more than 22000 s.

The number of population and generation should be chosen according to the need to obtain the greatest number of results versus the time taken, but it should be verified by means of several simulations that the results obtained are repeatable and therefore representative.

It can be seen that if a very low number of population and generation is chosen to reduce the computation time, the solutions of each simulation can differ greatly, as can be seen in the case of $Pop = 100$,

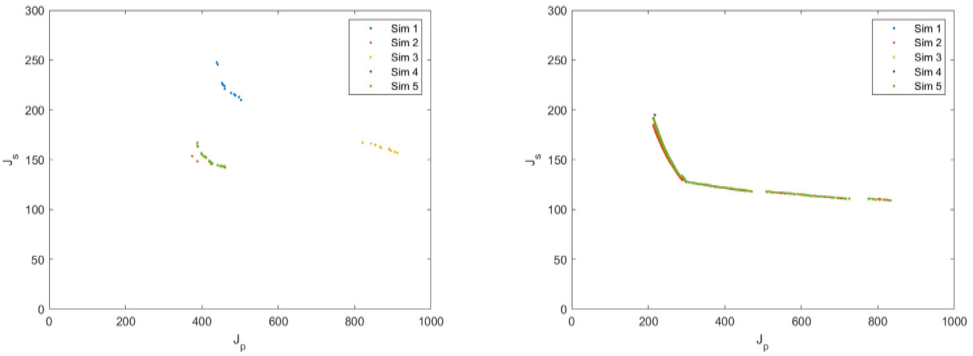

(a) $Pop = 100$, $Gen = 100$ (b) $Pop = 2000$, $Gen = 2000$

Fig. 9. Pareto-Fronts obtained in the five simulations of cases (a) $Pop = 100$, $Gen = 100$ and (b) $Pop = 2000$, $Gen = 2000$.

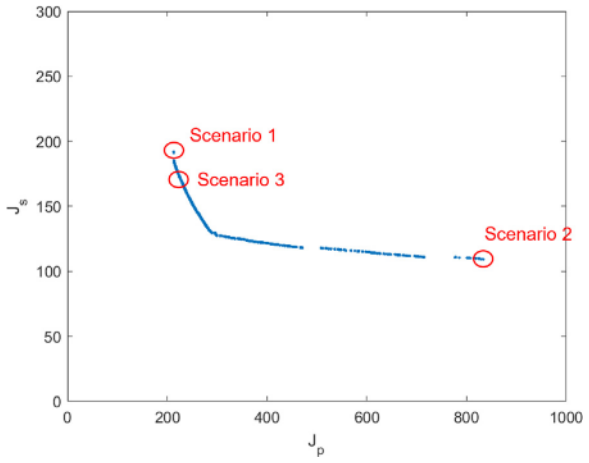

Fig. 10. Scenarios.

$Gen = 100$ in Fig. 9(a). In comparison, the solutions of the 5 simulations for the case $Pop = 2000$, $Gen = 2000$ are practically the same, as can be seen in Fig. 9(b). Therefore, for the case study, the results for the $Pop = 100$, $Gen = 100$ case cannot be considered valid.

6. Verification of the systems obtained

The validation of the results obtained by equations has been carried out by comparing with the Matlab-Simulink model, where the battery is replaced by the optimal value of the controlled secondary voltage V_s. In Chang, Quan, Zhu, Zong, and Zhou (2014), Zhu, Liu, Yu, Ma, and Cheng (2008) has been adequately modelled using various simulation programs.

For this purpose, three solutions obtained from the Pareto-Set of the case $Pop = 2000$, $Gen = 2000$ have been selected, according to the three scenarios previously defined in Section 2 (Fig. 10

- Scenario 1: Minimisation of copper from the shore, minimisation of J_p.
- Scenario 2: Minimisation of copper from on-board coil, minimisation of J_s.
- Scenario 3: Balanced joint copper minimisation of both coils, minimisations of $J_p + J_s$.

Table 10 shows the values of the primary and secondary parameters of the selected individuals based on each scenario, as well as the copper volume.

Table 10
Scenarios.

Sce	$Vol\ Cu_p$ (cm^3)	$Vol\ Cu_s$ (cm^3)	S_p (mm^2)	N_p	S_s (mm^2)	N_s	V_p (V)	V_2 (V)
1	221.56	195.15	23.41	9	30.74	10	209.98	268.42
2	870.95	122.64	79.94	12	18.5	10	332.15	229.49
3	243.47	178.17	23.39	10	30.56	9	215.74	270.14

Table 11
Scenario 1.

	Equation	Simulink	Error (%)
I_p (A)	46.81	47.24	−0.91
I_s (A)	58.17	58.19	−0.03
VC_p (V)	2618	2642	−0.91
VC_s (V)	1870.4	1871	−0.03
P_s (kW)	10.98	11	−0.12

Table 12
Scenario 2.

	Equation	Simulink	Error (%)
I_p (A)	54.59	54.9	−0.57
I_s (A)	36.79	36.81	−0.06
VC_p (V)	3236.1	3254	−0.55
VC_s (V)	1420.7	1421	−0.02
P_s (kW)	10.99	10.99	0

Table 13
Scenario 3.

	Equation	Simulink	Error (%)
I_p (A)	46.49	46.9	−0.87
I_s (A)	56.61	56.64	−0.04
VC_p (V)	3071.1	3098	−0.87
VC_s (V)	1578.1	1578	0.01
P_s (kW)	10.987	11	−0.12

Tables 11–13 show the value of the primary and secondary currents, as well as the voltages in the primary and secondary capacitors obtained by means of the mathematical equations of the model and by simulation with Matlab-Simulink. As can be seen, the error is less than 0.65% in the worst case.

7. Conclusion

This paper presents an optimal design procedure for an 11 kW S-S WPT system complying with SAE J2954 standard. The procedure involves the utilisation of improved mathematical modelling of electrical variables and the equivalent electrical circuit, along with the development of a NSGA-II genetic algorithm and the secant method.

Firstly, an equation-based method for calculating the resistances and inductances of the circuit has been presented. Secondly, a NSGA-II

genetic algorithm has been proposed for the optimisation of the coils and capacitors of the resonant circuit.

The mathematical approach provides results comparable to those obtained through finite element analysis. Moreover, it significantly reduces calculation times compared to finite elements, and facilitates its integration into the NSGA-II genetic algorithm, thereby simplifying and accelerating the calculation process.

The proposed NSGA-II genetic algorithm employs two opposing objective functions and encompasses three distinct optimisation scenarios. The objective functions focus on minimising the copper volume in the primary coil and the copper volume in the secondary coil.

As a result, three different solutions are obtained, one for each scenario, all of which satisfy the requirements of the SAE J2954 Standard. The result obtained in Scenario 1 requires the least amount of copper in the primary. Scenario 2 minimises copper in the secondary, which is half the amount needed in Scenario 1, at the cost of significantly increasing the copper required in the primary. Finally, Scenario 3 achieves the intermediate compromise, minimising the combined volume of copper in both coils, resulting in the lowest combined cost.

The three WPT designs have been validated by first checking the results obtained by equations and checking the behaviour according to expectations by simulation in Matlab-Simulink.

The proposed method can be easily adapted to other objective functions and constraints, allowing solutions tailored to specific requirements. Furthermore, it can be applied to any other WPT topology by substituting the equations in Section 2 and incorporating them into Step 2 of the NSGA-II algorithm.

CRediT authorship contribution statement

O. García-Izquierdo: Conceptualization, Methodology, Software, Visualization, Investigation, Analysis formal, Writing – original draft. **J.F. Sanz:** Conceptualization, Resources, Writing – original draft, Writing – review & editing, Visualization, Supervision, Project administration, Funding acquisition. **J.L. Villa:** Conceptualization, Supervision, Validation, Resources, Writing – review & editing. **G. Martin-Segura:** Validation, Resources.

Data availability

No data was used for the research described in the article

Acknowledgements

This research project has been partially sponsored by the Spanish research project Misiones CDTI - Movilidad2030 (MIG-20201040).

References

Abid, M. S., Ahshan, R., Al-Abri, R., Al-Badi, A., & Albadi, M. (2023). Multi-objective optimal planning of virtual synchronous generators in microgrids with integrated renewable energy sources. *IEEE Access*, *11*, 65443–65456. http://dx.doi.org/10.1109/ACCESS.2023.3289813.

Abunike, E., Okoro, O., & Davidson, I. (2021). Finite element design and multi-objective optimization of four pole reluctance motor based on NSGA-II intelligent algorithm. (pp. 1–6). http://dx.doi.org/10.1109/AFRICON51333.2021.9570964.

Acero, J., Carretero, C., Lope, I., Alonso, R., & Burdío, J. (2016). Analytical solution of the induced currents in multilayer cylindrical conductors under external electromagnetic sources. *Applied Mathematical Modelling*, *40*, http://dx.doi.org/10.1016/j.apm.2016.07.031.

Aebischer, H. A. (2018). Comparative study of the accuracy of analytical inductance formulae for square planar spiral inductors. *Advanced Electromagnetics*, *7*(5), 37–48. http://dx.doi.org/10.7716/aem.v7i5.862, URL http://aemjournal.org/index.php/AEM/article/view/862.

Aebischer, H. A. (2019). Inductance formula for square spiral inductors with rectangular conductor cross section. *Advanced Electromagnetics*, *8*(4), 80–88. http://dx.doi.org/10.7716/aem.v8i4.1074, URL http://aemjournal.org/index.php/AEM/article/view/1074.

Aebischer, H. A. (2020). Inductance formula for rectangular planar spiral inductors with rectangular conductor cross section. *Advanced Electromagnetics*, *9*(1), 1–18. http://dx.doi.org/10.7716/aem.v9i1.1346, URL http://aemjournal.org/index.php/AEM/article/view/1346.

Aebischer, H. A., & Aebischer, B. (2014). Improved formulae for the inductance of straight wires. *Advanced Electromagnetics*, *3*(1), 31–43. http://dx.doi.org/10.7716/aem.v3i1.254, URL http://aemjournal.org/index.php/AEM/article/view/254.

Ahmed, F., Zhu, S., Yu, G., & Luo, E. (2022). A potent numerical model coupled with multi-objective NSGA-II algorithm for the optimal design of stirling engine. *Energy*, *247*, Article 123468. http://dx.doi.org/10.1016/j.energy.2022.123468.

Aydin, E., Aydemir, M. T., Aksoz, A., El Baghdadi, M., & Hegazy, O. (2022). Inductive power transfer for electric vehicle charging applications: A comprehensive review. *Energies*, *15*(14), http://dx.doi.org/10.3390/en15144962, URL https://www.mdpi.com/1996-1073/15/14/4962.

Balasubramanian, L., Bhuiyan, N. A., Javied, A., Fahmy, A. A., Belblidia, F., & Sienz, J. (2023). Design and optimization of interior permanent magnet (IPM) motor for electric vehicle applications. *CES Transactions on Electrical Machines and Systems*, *7*(2), 202–209. http://dx.doi.org/10.30941/CESTEMS.2023.00021.

Bertoluzzo, M., Di Barba, P., Forzan, M., Mognaschi, M. E., & Sieni, E. (2021). Multiobjective optimization of compensation networks for wireless power transfer systems. *COMPEL - The International Journal for Computation and Mathematics in Electrical and Electronic Engineering*, *ahead-of-print*, http://dx.doi.org/10.1108/COMPEL-06-2021-0204.

Beyer, H.-G., & Deb, K. (2001). On self-adaptive features in real-parameter evolutionary algorithms. *IEEE Transactions on Evolutionary Computation*, *5*, 250–270.

Blažek, V., Prokop, L., Misak, S., Kedron, P., & Pergl, I. (2023). Impact of energy consumption optimisation on the electrical self-sufficiency of a microgrid with vehicle-to-grid technology. (pp. 279–283). http://dx.doi.org/10.1109/ECTIDAMTNCON57770.2023.10139540.

Bosshard, R., & Kolar, J. W. (2016). Multi-Objective Optimization of 50 kW/85 kHz IPT System for Public Transport. *IEEE Journal of Emerging and Selected Topics in Power Electronics*, *4*(4), 1370–1382. http://dx.doi.org/10.1109/JESTPE.2016.2598755.

Chacón, J., & Segura, C. (2018). Analysis and enhancement of simulated binary crossover. In *2018 IEEE congress on evolutionary computation* (pp. 1–8). http://dx.doi.org/10.1109/CEC.2018.8477746.

Chang, R., Quan, L., Zhu, X., Zong, Z., & Zhou, H. (2014). Design of a wireless power transfer system for EV application based on finite element analysis and MATLAB simulation. In *2014 IEEE conference and expo transportation electrification Asia-Pacific* (pp. 1–4). http://dx.doi.org/10.1109/ITEC-AP.2014.6941225.

Chen, Y., Zhang, H., Shin, C.-S., Seo, K.-H., Park, S.-J., & Kim, D.-H. (2019). A comparative study of S-S and LCC-s compensation topology of inductive power transfer systems for EV chargers. In *2019 IEEE 10th international symposium on power electronics for distributed generation systems* (pp. 99–104). http://dx.doi.org/10.1109/PEDG.2019.8807684.

Cirimele, V., Torchio, R., Villa, J. L., Freschi, F., Alotto, P., Codecasa, L., et al. (2020). Uncertainty quantification for SAE J2954 compliant static wireless charge components. *IEEE Access*, *8*, 171489–171501. http://dx.doi.org/10.1109/ACCESS.2020.3025052.

Deb, K., & Agrawal, R. B. (1995). Simulated binary crossover for continuous search space. *Complex Systems*, *9*.

Deb, K., & Kumar, A. (1995). Real-coded genetic algorithms with simulated binary crossover: Studies on multimodal and multiobjective problems. *Complex Systems*, *9*.

Deb, K., Pratap, A., Agarwal, S., & Meyarivan, T. (2002). A fast and elitist multiobjective genetic algorithm: NSGA-II. *IEEE Transactions on Evolutionary Computation*, *6*(2), 182–197. http://dx.doi.org/10.1109/4235.996017.

Ding, Y., Yang, C., & Xiong, B. (2021). Multi-objective optimal design of traction transformer using improved NSGA-II. In *2021 24th international conference on electrical machines and systems* (pp. 1470–1474). http://dx.doi.org/10.23919/ICEMS52562.2021.9634516.

El-Nemr, M., Afifi, M., Rezk, H., & Ibrahim, M. (2021). Finite element based overall optimization of switched reluctance motor using multi-objective genetic algorithm (NSGA-II). *Mathematics*, *9*(5), http://dx.doi.org/10.3390/math9050576, URL https://www.mdpi.com/2227-7390/9/5/576.

Greenhouse, H. (1974). Design of planar rectangular microelectronic inductors. *IEEE Transactions on Parts, Hybrids, and Packaging*, *10*(2), 101–109. http://dx.doi.org/10.1109/TPHP.1974.1134841.

Guillod, T., Huber, J., Krismer, F., & Kolar, J. W. (2017). Litz wire losses: Effects of twisting imperfections. In *2017 IEEE 18th workshop on control and modeling for power electronics* (pp. 1–8). http://dx.doi.org/10.1109/COMPEL.2017.8013327.

Hasan, N., Yilmaz, T., Zane, R., & Pantic, Z. (2015). Multi-objective particle swarm optimization applied to the design of Wireless Power Transfer systems. In *2015 IEEE wireless power transfer conference* (pp. 1–4). http://dx.doi.org/10.1109/WPT.2015.7139138.

Heydari, A., Keynia, F., Fekih, A., Bertling Tjernberg, L., Barchi, G., & Moser, D. (2023). A new combined PV output power forecasting model based on optimized LSTM network. (pp. 1–6). http://dx.doi.org/10.1109/GlobConET56651.2023.10149975.

Jinliang, L., Qijun, D., Wenshan, H., & Hong, Z. (2017). Research on quality factor of the coils in wireless power transfer system based on magnetic coupling resonance. In *2017 IEEE PELS workshop on emerging technologies: Wireless power transfer* (pp. 123–127). http://dx.doi.org/10.1109/WoW.2017.7959378.

Jung, D., Choi, Y. H., & Kim, J. H. (2017). Multiobjective automatic parameter calibration of a hydrological model. *Water*, *9*(3), http://dx.doi.org/10.3390/w9030187, URL https://www.mdpi.com/2073-4441/9/3/187.

Li, J., Tan, L., Huang, X., Wang, R., & Zhang, M. (2020). The influence of substrate size changes on the coil resistance of the wireless power transfer system. *Electronics*, *9*(6), http://dx.doi.org/10.3390/electronics9061025, URL https://www.mdpi.com/2079-9292/9/6/1025.

Li, X., & Xia, C. (2021). Multi-objective optimization of ADRC parameters for constant voltage output in ICPT systems based on NSGA-II. In *2021 6th Asia conference on power and electrical engineering* (pp. 1403–1407). http://dx.doi.org/10.1109/ACPEE51499.2021.9437047.

Liu, D., Wei, B., Cai, C., & Yuan, W. (2020). Optimization design of amorphous metal distribution transformer based on improved fast and elitist multi-objective genetic algorithm. In *2020 IEEE international conference on high voltage engineering and application* (pp. 1–4). http://dx.doi.org/10.1109/ICHVE49031.2020.9279947.

Low, Z. N., Chinga, R. A., Tseng, R., & Lin, J. (2009). Design and test of a high-power high-efficiency loosely coupled planar wireless power transfer system. *IEEE Transactions on Industrial Electronics*, *56*(5), 1801–1812. http://dx.doi.org/10.1109/TIE.2008.2010110.

Luo, Z., Wei, X., & Covic, G. A. (2018). Multi-objective Optimization of double D coils for wireless charging system. In *2018 IEEE international power electronics and application conference and exposition* (pp. 1–6). http://dx.doi.org/10.1109/PEAC.2018.8589975.

Ma, H., Zhang, Y., Sun, S., Liu, T., & Shan, Y. (2023). A comprehensive survey on NSGA-II for multi-objective optimization and applications. *Artificial Intelligence Review*, 1–54. http://dx.doi.org/10.1007/s10462-023-10526-z.

Mohammadi, A. S., Trovão, J. P. F., & Antunes, C. H. (2020). Component-level optimization of hybrid excitation synchronous machines for a specified hybridization ratio using NSGA-II. *IEEE Transactions on Energy Conversion*, *35*(3), 1596–1605. http://dx.doi.org/10.1109/TEC.2020.2990283.

Movagharnejad, H., & Mertens, A. (2017). Design metrics of compensation methods for contactless charging of electric vehicles. In *2017 19th European conference on power electronics and applications* (pp. P.1–P.10). http://dx.doi.org/10.23919/EPE17ECCEEurope.2017.8099403.

Otomo, Y., & Igarashi, H. (2019). A 3-D topology optimization of magnetic cores for wireless power transfer device. *IEEE Transactions on Magnetics*, *55*(6), 1–5. http://dx.doi.org/10.1109/TMAG.2019.2900744.

Pan, Z., & Fang, S. (2022). Combined random forest and NSGA-II for optimal design of permanent magnet arc motor. *IEEE Journal of Emerging and Selected Topics in Power Electronics*, *10*(2), 1800–1812. http://dx.doi.org/10.1109/JESTPE.2021.3049242.

Paul, A. K. (2018). Current density characterization of litz wires used in induction heating coils: A practical approach. In *2018 IEEE international conference on power electronics, drives and energy systems* (pp. 1–6). http://dx.doi.org/10.1109/PEDES.2018.8707901.

Pei, Y., Pichon, L., Le Bihan, Y., Bensetti, M., & Dessante, P. (2022). Fast shielding optimization of an inductive power transfer system for electric vehicles. *IEEE Access*, *10*, 91227–91234. http://dx.doi.org/10.1109/ACCESS.2022.3198953.

Pétrowski, A., & Ben Hamida, S. (2017). Multi-objective optimization. (pp. 165–182). http://dx.doi.org/10.1002/9781119136378.ch5.

Raghuwanshi, M. M., Kakde, O. G., & Gandhi, R. (2004). Survey on multiobjective evolutionary and real coded genetic algorithms.

Ranjan, S., & Mishra, S. (2015). Multi-objective design optimization of three-phase induction motor using NSGA-II algorithm. *32*, (pp. 1–8). http://dx.doi.org/10.1007/978-81-322-2208-8_1,

Sallan, J., Villa, J. L., Llombart, A., & Sanz, J. F. (2009). Optimal design of ICPT systems applied to electric vehicle battery charge. *IEEE Transactions on Industrial Electronics*, *56*(6), 2140–2149. http://dx.doi.org/10.1109/TIE.2009.2015359.

Shahryari, E., Shayeghi, H., & Moradzadeh, M. (2018). Probabilistic and multi-objective placement of D-STATCOM in distribution systems considering load uncertainty. *Electric Power Components and Systems*, *46*, 1–16. http://dx.doi.org/10.1080/15325008.2018.1431819.

Shevchenko, V., Husev, O., Strzelecki, R., Pakhaliuk, B., Poliakov, N., & Strzelecka, N. (2019). Compensation topologies in IPT systems: Standards, Requirements, classification, analysis, comparison and application. *IEEE Access*, *7*, 120559–120580. http://dx.doi.org/10.1109/ACCESS.2019.2937891.

Sinha, A. (2011a). *Progressively interactive evolutionary multiobjective optimization* (Ph.D. thesis), (p. vi, 129 s.). Aalto University, School of Business, URL http://urn.fi/URN:ISBN:978-952-60-4052-3.

Sinha, A. (2011b). Bilevel multi-objective optimization problem solving using progressively interactive EMO. In R. H. C. Takahashi, K. Deb, E. F. Wanner, & S. Greco (Eds.), *Evolutionary multi-criterion optimization* (pp. 269–284). Berlin, Heidelberg: Springer Berlin Heidelberg.

Stadler, A. (2013). The optimization of high frequency inductors with litz-wire windings. In *2013 International conference-workshop compatibility and power electronics* (pp. 209–213). http://dx.doi.org/10.1109/CPE.2013.6601156.

Tan, K., Lee, T., & Khor, E. (2001). Evolutionary algorithms for multi-objective optimization: Performance assessments and comparisons. In *Proceedings of the 2001 congress on evolutionary computation (IEEE Cat. No.01TH8546), Vol. 2* (pp. 979–986). http://dx.doi.org/10.1109/CEC.2001.934296.

Tan, L., Tang, Z., Zhong, R., Huang, X., Liu, H., & Chen, C. (2019). An optimization strategy based on dimension reduction method in wireless charging system design. *IEEE Access*, *7*, 151733–151745. http://dx.doi.org/10.1109/ACCESS.2019.2948196.

Tourkhani, F., & Viarouge, P. (2001). Accurate analytical model of winding losses in round Litz wire windings. *IEEE Transactions on Magnetics*, *37*(1), 538–543. http://dx.doi.org/10.1109/20.914375.

Verma, S., Pant, M., & Snášel, V. (2021). A comprehensive review on NSGA-II for multi-objective combinatorial optimization problems. *IEEE Access*, *9*, 57757–57791.

Villa, J., Llombart, A., Sanz, J., & Sallan, J. (2007). Practical development of a 5 kW ICPT System SS compensated with a large air gap. In *2007 IEEE international symposium on industrial electronics* (pp. 1219–1223). http://dx.doi.org/10.1109/ISIE.2007.4374772.

Villa, J. L., Sallán, J., Llombart, A., & Sanz, J. F. (2009). Design of a high frequency inductively coupled power transfer system for electric vehicle battery charge. *Applied Energy*, *86*(3), 355–363. http://dx.doi.org/10.1016/j.apenergy.2008.05.009, URL https://www.sciencedirect.com/science/article/pii/S0306261908001359.

Villa, J. L., Sallan, J., Sanz Osorio, J. F., & Llombart, A. (2012). High-misalignment tolerant compensation topology for ICPT systems. *IEEE Transactions on Industrial Electronics*, *59*(2), 945–951. http://dx.doi.org/10.1109/TIE.2011.2161055.

Wang, C.-S., Covic, G., & Stielau, O. (2001). General stability criterions for zero phase angle controlled loosely coupled inductive power transfer systems. In *IECON'01. 27th Annual conference of the IEEE industrial electronics society (Cat. No.37243), Vol. 2* (pp. 1049–1054). http://dx.doi.org/10.1109/IECON.2001.975925.

Wang, C., Han, W., Chen, P., Song, J., & Yuan, S. (2022). Multiobjective optimization design of high frequency transformer based on NSGA-II algorithm. In *2022 IEEE international conference on mechatronics and automation* (pp. 664–669). http://dx.doi.org/10.1109/ICMA54519.2022.9856127.

Wang, Q., Li, S., Ding, H., Cheng, M., & Buja, G. (2023). Planning of DC electric spring with particle swarm optimization and elitist non-dominated sorting genetic algorithm. *CSEE Journal of Power and Energy Systems*, 1–10. http://dx.doi.org/10.17775/CSEEJPES.2022.04510.

(2020). *Wireless power transfer for light-duty plug-in/electric vehicles and alignment methodology*: *Standard*.

Woodworth, A. A., Smith, A., Sixel, W., Edwards, R., Jansen, R., McCormick, S., et al. (2019). Thermal analysis of potted litz wire for high-power-density aerospace electric machines. In *2019 AIAA/IEEE electric aircraft technologies symposium* (pp. 1–13). http://dx.doi.org/10.2514/6.2019-4509.

Xu, L., Zhu, X., Zhang, C., Zhang, L., & Quan, L. (2021). Power oriented design and optimization of dual stator linear-rotary generator with Halbach PM array for ocean energy conversion. *IEEE Transactions on Energy Conversion*, *36*(4), 3414–3426. http://dx.doi.org/10.1109/TEC.2021.3070633.

Yan, X.-Y., Yang, S.-C., He, H., & Tang, T.-Q. (2018). An optimization model for wireless power transfer system based on circuit simulation. *Physica A. Statistical Mechanics and its Applications*, *509*(C), 873–880. http://dx.doi.org/10.1016/j.physa.2018.06.0.

Yang, J., Liu, R., Tong, Q., Yang, X., Liu, Q., & Yao, A. (2023). Multi-objective optimization of LCC-s-compensated IPT system for improving misalignment tolerance. *Applied Sciences*, *13*(6), http://dx.doi.org/10.3390/app13063666, URL https://www.mdpi.com/2076-3417/13/6/3666.

Yao, Y., Wang, Y., Liu, X., Pei, Y., Xu, D., & Liu, X. (2019). Particle swarm optimization-based parameter design method for S/CLC-compensated IPT systems featuring high tolerance to misalignment and load variation. *IEEE Transactions on Power Electronics*, *34*(6), 5268–5282. http://dx.doi.org/10.1109/TPEL.2018.2870530.

Yilmaz, T., Hasan, N., Zane, R., & Pantic, Z. (2017). Multi-objective optimization of circular magnetic couplers for wireless power transfer applications. *IEEE Transactions on Magnetics*, *53*(8), 1–12. http://dx.doi.org/10.1109/TMAG.2017.2692218.

Zhang, D., Liu, J., Jiao, S., Tian, H., Lou, C., Zhou, Z., et al. (2019). Research on the configuration and operation effect of the hybrid solar-wind-battery power generation system based on NSGA-II. *Energy*, *189*, Article 116121. http://dx.doi.org/10.1016/j.energy.2019.116121.

Zhang, W., & Mi, C. C. (2016). Compensation topologies of high-power wireless power transfer systems. *IEEE Transactions on Vehicular Technology*, *65*(6), 4768–4778. http://dx.doi.org/10.1109/TVT.2015.2454292.

Zhang, R., Moreira, M., & Corte-Real, J. (2015). Multi-objective calibration of the physically based, spatially distributed SHETRAN hydrological model. *Journal of Hydroinformatics*, *18*(3), 428–445. http://dx.doi.org/10.2166/hydro.2015.219, arXiv:https://iwaponline.com/jh/article-pdf/18/3/428/478800/jh0180428.pdf.

Zhu, C., Liu, K., Yu, C., Ma, R., & Cheng, H. (2008). Simulation and experimental analysis on wireless energy transfer based on magnetic resonances. In *2008 IEEE Vehicle power and propulsion conference* (pp. 1–4). http://dx.doi.org/10.1109/VPPC.2008.4677400.

Zitzler, E., Brockhoff, D., & Thiele, L. (2007). The hypervolume indicator revisited: On the design of Pareto-compliant indicators via weighted integration. In S. Obayashi, K. Deb, C. Poloni, T. Hiroyasu, & T. Murata (Eds.), *Evolutionary multi-criterion optimization* (pp. 862–876). Berlin, Heidelberg: Springer Berlin Heidelberg.

Zitzler, E., Deb, K., & Thiele, L. (2000). Comparison of multiobjective evolutionary algorithms: empirical results. *Evolutionary Computation*, *8*(2), 173–195. http://dx.doi.org/10.1162/106365600568202.